Journal of Crystal Growth 576 (2021) 126362

Contents lists available at ScienceDirect

Journal of Crystal Growth

journal homepage: www.elsevier.com/locate/jcrysgro

Real-time investigation of Lysozyme crystallization kinetics: A neutron diffraction study

M. Longo, R.J. Heigl, T.E. Schrader *

Forschungszentrum Jülich GmbH, Jülich Centre for Neutron Science (JCNS) at Heinz Maier-Leibnitz Zentrum (MLZ), Lichtenbergstrasse 1, 85748 Garching, Germany

ARTICLE INFO

Communicated by Alexander van Driessche

Keywords:
A1. Biocrystallization
A2. Growth from solutions
B1. Lysozyme
B1. Biological macromolecules

ABSTRACT

The isothermal crystallization kinetics of hen-egg-white Lysozyme has been investigated by means of a time-resolved neutron diffraction experiment for almost 3 days, starting from a supersaturated solution of Lysozyme (30 mg/ml, 3 wt% NaCl, pD 4.75 at 298 K) until the growth of crystals, in order to have complementary information about the crystallization kinetics (Heigl et al., 2018). The temporal evolution of the intensity of the Bragg peaks, observed in the neutron diffraction images when a single crystal appears, has been studied. Simultaneously, the analysis of the small angle neutron scattering curves from the Lysozyme solution, during the crystallization process, has been performed. A correlated behaviour between the decrease of the Lysozyme concentration and the increase of the crystallization fraction was observed. The crystallization kinetics was described by means of the Johnson-Mehl-Avrami-Kolmogorov model and parameters compatible with our previous Lysozyme crystallization study have been found.

The Lysozyme crystallization under constant neutron flux underlines the known strength of neutrons in studying biological samples without causing radiation damage.

1. Introduction

Despite the great advances obtained in Cryo-Electron Microscopy [2], crystallographic techniques are still the main method used to obtain the three-dimensional structure of biological macromolecules at atomic resolution. Both X-ray and neutron diffraction require the growth of high-quality crystals, which is the most important step to overcome for both techniques. Because of the key role of hydrogen and water molecules in many physiological functions of biological macromolecules, neutron crystallography provides a powerful complement even to high resolution X-ray crystallography and Cryo-Electronmicroscopy, when hydrogen atoms are of special interest. Unfortunately, electrons (in case of Cryo-elecronmicroscopy) and X-rays are scattered mostly by the electrons of the atoms of the sample of which hydrogen only posseses one. Neutrons are scattered from the nuclei and the neutron scattering length of hydrogen and deuterium is comparable to that of other elements. Therefore, their location can be directly determined, even at moderate resolution (2.5 Å). Due to the lower flux of the neutron beam, sufficiently large crystals are necessary (0.1–0.5 mm^3) to perform an experiment in a reasonable amount of time (typically 5–15 days). In this context, an understanding of the crystallization process is essential to improve and control the crystal growth. So far, many efforts have been made in this respect by using different experimental techniques such as small angle scattering, static and dynamic light scattering and transmission electron microscopy in order to take into account for the many different size ranges which are developing from the nucleation until the crystal growth [1,3–5]. Because of the resolution limit, optical microscopy cannot give information about the nucleation process in the early stage of the crystallization. Even neutron backscattering and spin-echo spectroscopy have been used in order to measure the pico- to nanosecond time scale diffusive dynamics in protein solutions during crystallization [6]. In this work, we investigated the crystallization kinetics of hen-egg-white-lysozyme by a neutron diffraction experiment at BIODIFF [7] (FRM II, Garching) starting from a supersaturated solution of hen-egg-white lysozyme until the achievement of the final crystals. We chose the same batch crystallization condition used in our previous work [1] in order to extend our results to wide and small angle neutron scattering measurements. The BIODIFF cylindrical neutron image plate allowed us to investigate at the same time both the temporal evolution of the Bragg peaks and the small angle neutron scattering (SANS) signal during the crystallization process. A similar attempt has been made by A. Sauter et al. [3] which used small angle X-ray scattering (SAXS) to study

* Corresponding author.
E-mail address: t.schrader@fz-juelich.de (T.E. Schrader).

https://doi.org/10.1016/j.jcrysgro.2021.126362
Received 4 January 2021; Received in revised form 22 September 2021; Accepted 27 September 2021
Available online 1 October 2021

the nucleation mechanism by following the evolution of Bragg peaks in the small angle scattering curves, radially averaged with respect to a constant 2θ scattering angle. In our work, because of the BIODIFF image plate, the origin of single Bragg peaks, related to single crystals growing in the neutron beam, has been observed. As neutrons are a non-destructive probe, a long measurement of ca. 60 h on the same sample has been performed continuously without any noticeable sample damage. It is well known that neutron scattering is not affected by radiation damage [8]. The sample was kept at the temperature of 298 K, close to the neutron guide hall a the FRM II in order to increase the protein solubility and slow down the crystallization. This also ensures comparability to the short term measurements shown in our previous work [1].

2. Sample preparation

The crystallization solution investigated in this work was obtained by a 1:1 mixture of a 60 mg/ml Lysozyme solution and a 6 wt% NaCl buffer. Both solutions were prepared in heavy water (D_2O) in order to reduce the incoherent scattering of neutrons [9] and a pD of 4.75 (pD = pH + 0.4) was chosen. As Lysozyme was directly dissolved in D_2O, the desired pD was achieved by adding the needed amount of a 1 M sodium acetate solution. The 6 wt% sodium chloride solution was prepared in a deuterated 5 mM sodium acetate/acetic acid buffer. To crystallize, the batch crystallization method was used: both solutions were injected in the sample holder. Before mixing, both solutions were filtered with a pore size of 0.02 μm. Quartz glass capillaries with a diameter of 4 mm were used as sample holder. Just after mixing of the lysozyme and buffer solutions, the capillary containing the sample solution was placed in the BIODIFF sample holder in order to start the neutron diffraction measurements. The temperature was constant during the experiment and was close to the temperature of the neutron guide hall (298 K).

3. Experimental set-up

The neutron diffraction experiment was performed using the BIODIFF instrument at the Heinz Maier-Leibnitz Zentrum (MLZ), a monochromatic diffractometer with a neutron image-plate detector using neutrons from the cold source of the Forschungs-Neutronenquelle Heinz Maier-Leibnitz (FRM II, Germany). Since the aim of the experiment was to study the time evolution of the diffraction pattern during the crystallization process, 88 frames were recorded with an exposure time of 2000 s each without any change of the orientation. The neutron wavelength was 4.213 Å. This wavelength was chosen in order to increase the q-resolution of the instrument BIODIFF in reciprocal space and to shift the accessible q-range to lower values. The momentum transfer in reciprocal space q is defined by

$$q = \frac{4\pi}{\lambda}\sin(\theta/2) \tag{1}$$

with the neutron wavelength λ and the scattering angle θ. The accessible q-range at the chosen wavelength was between 0.067 $Å^{-1}$ and 2.98 $Å^{-1}$.

4. Results and discussion

At the beginning the sample was made up of just mixed Lysozyme and buffer solutions inside a quartz capillary at the temperature of the experimental hall at FRM II (298 K). At the end of the experiment at the position where the neutron beam penetrated the capillary a large Lysozyme crystal was found stuck to the inner capillary surface, surrounded by the solution. Some more crystals were seen outside the neutron beam area, also stuck to the glass wall of the capillary. At the end of the experiment at the position where the neutron beam penetrated the capillary a large Lysozyme crystal was found stuck to the inner capillary surface, surrounded by the solution. Some more crystals were seen outside the neutron beam area, also stuck to the glass wall of the capillary. In Fig. 2, a comparison between the initial (t = 0.55 h) and the final (t = 60.78 h) diffraction neutron image pattern of the sample can be observed. The final collected data were indexed using the HKL-2000 program suite [10]. The crystal belonged to space group $P4_32_12$ with the unit cell parameters $a = b = 79.5$ Å, $c = 37.8$ Å and $\alpha = \beta = \gamma = 90°$ [11]. Due to the cylindrical detector geometry of the BIODIFF detector, which is not optimized for small angle experiments, radial averaging of the small angle signal was discarded. Instead, a narrow horizontal strip (90 detector pixel high, one pixel corresponds to a square of 250 μm) passing through the center of the scattered signal and perpendicular to the axis of the cylindrical detector has been selected (See yellow box in Fig. 1). In this way, a simultaneous evaluation of the SANS signal was possible together with the analysis of the temporal evolution of the indexed Bragg peaks. The selected section has been integrate by means of the ProfilePlot package of the open source program ImageJ [12] in order to get the SANS signal of the selected area for each of the 88 recorded frames. Along the direction of the integrated strip, a conversion from pixel to the scattering angle θ is quite easy:

$$\theta = \frac{pixel_i}{pixel_{tot}}\cdot 180° \tag{2}$$

where $pixel_i$ is the i-th pixel number and $pixel_{tot}$ is the total number of pixels in the horizontal axis of the image strip. The same horizontal strip has been used to extract the neutron small angle signal of the empty cell (the quartz capillary containing the sample), a Vanadium rod, a LiF sample as beam stop and of the buffer solution. The buffer solution was contained in a quartz capillary analogous to that used for the Lysozyme solution. These additional measurements were essential to obtain the macroscopic cross section of the small angle signal. Vanadium has been used as flat scatterer because of its high incoherent cross section, LiF has been chosen as absorber to estimate the background, and the buffer solution is measured to subtract the coherent and incoherent scattering coming from the solvent and the empty cell [13]. Based on this consideration, the calculation to obtain the macromolecular cross section of the sample is based on the following equation:

$$\left.\frac{d\Sigma(q)}{d\Omega}\right|_S = \left.\frac{d\Sigma(q)}{d\Omega}\right|_V \frac{\left(\frac{\Delta I(q)|_S - \Delta I(q)|_{LiF}}{Tr_S}\right) - \left(\frac{\Delta I(q)|_{Buffer} - \Delta I(q)|_{LiF}}{Tr_{Buffer}}\right)}{\left(\frac{\Delta I(q)|_V - \Delta I(q)|_{LiF}}{Tr_V}\right)} \tag{3}$$

where $\Delta I(q)|_S, \Delta I(q)|_{Buffer}, \Delta I(q)|_{LiF}$ and $\Delta I(q)|_V$ are the measured intensities of the sample (Lysozyme solution), the buffer solution, the absorber (LiF) and the flat scatterer (Vanadium). A flat scatterer scatters neutrons isotropically into all directions of space. It is therefore used to compensate detector inhomogeneities and to calibrate the measured scattering intensity with respect to an absolute scale. $Tr_S = 0.78$, $Tr_{Buffer} = 0.8$ and $Tr_V = 0.6$are the measured transmissions related to the sample, the empty cell and the Vanadium, respectively. Both the intensities from the sample and the buffer solution include the scattering from the quartz capillary as well. By using Eq. 3, a direct subtraction of both the solvent (buffer solution) and the empty cell contributions is performed. In order to estimate the differential cross section of Vanadium $\left.\frac{d\Sigma(q)}{d\Omega}\right|_V$, the following equation has been used:

$$\left.\frac{d\Sigma(q)}{d\Omega}\right|_V = \frac{\rho_V \sigma_{V,inc}}{4\pi} \tag{4}$$

where $\rho_V = d_V N_A / M_V, d_V$ is the mass density, N_A is the Avogadro's number and M_V is the molecular mass of Vanadium. These values are taken from literature [14] as $\sigma_{V,inc} = 5.08\cdot 10^{-24} cm^2$, $d_V = 5.8 g\cdot cm^{-3}$ and $M_V = 50.94 g/mol$. Therefore, $\left.\frac{d\Sigma(q)}{d\Omega}\right|_V = 0.0278 cm^{-1}$. The pictures in Fig. 2 show the diffracted neutron intensities measured on the BIODIFF neutron image plate at the intial time t = 0.55 h, when the sample is still

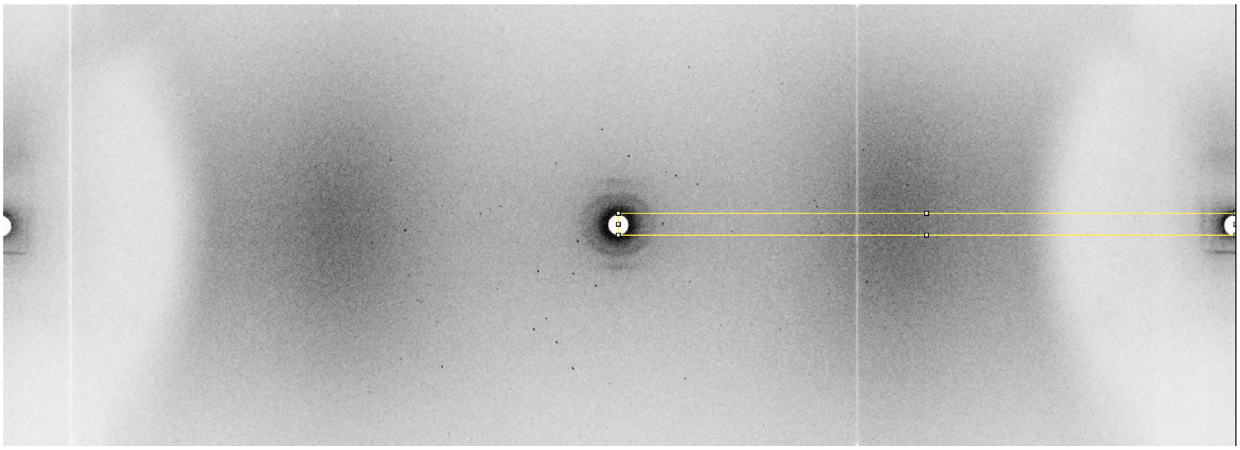

Fig. 1. Neutron diffraction image, at t = 60.78 h. The yellow rectangle describes the strip where the scattering signal has been integrated to obtain the small angle scattering curve. (For interpretation of the references to color in this figure legend, the reader is referred to the web version of this article.)

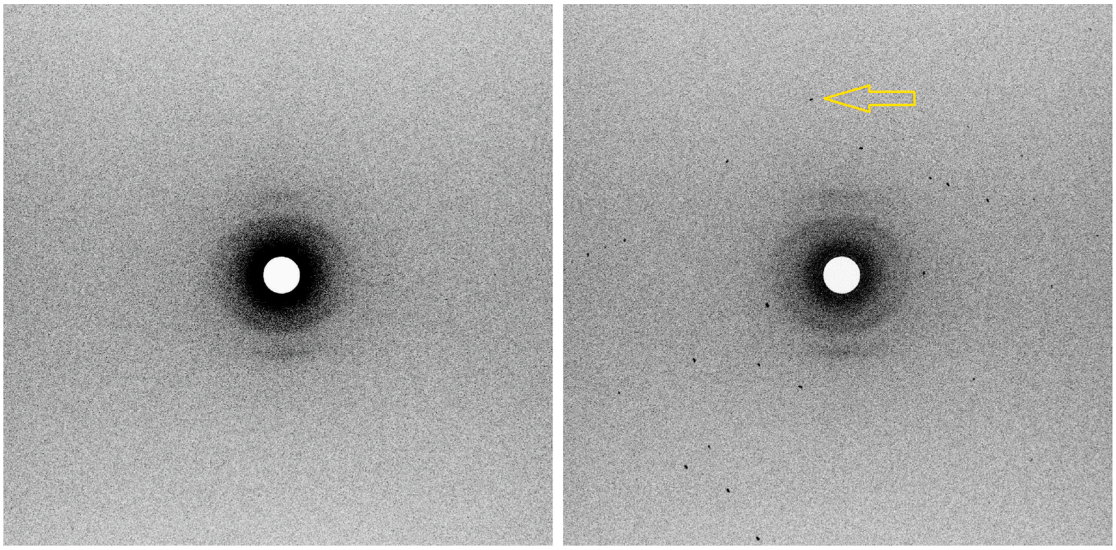

Fig. 2. Neutron diffraction image, close to the beamstop, at t = 0.55 h (left), where the sample is still a clear solution, and at t = 60.78 h (right), where Bragg peaks, due to the formation of the single crystal, can be observed. The yellow arrow points to the [2,−1,4] Bragg peak, whose intensity has been evaluated during the crystallization. (For interpretation of the references to color in this figure legend, the reader is referred to the web version of this article.)

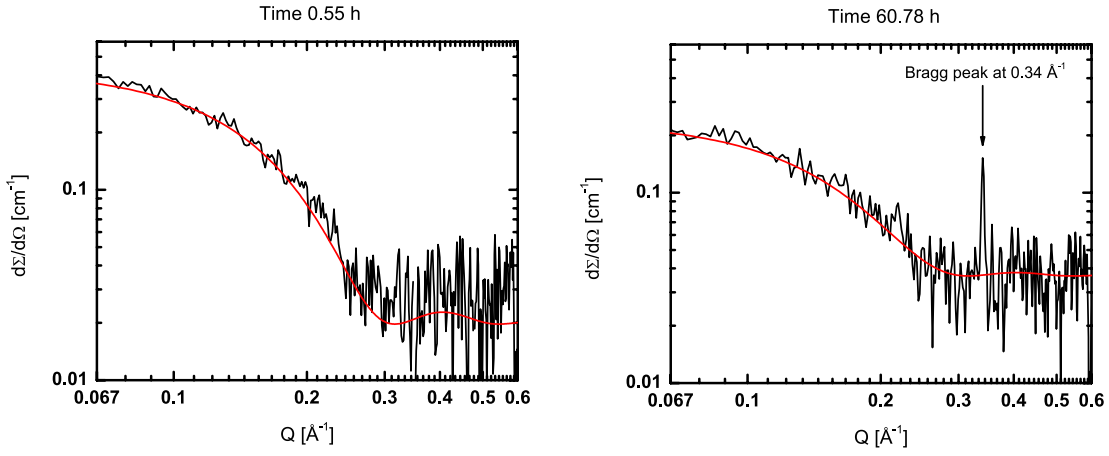

Fig. 3. SANS curves for 30 mg/ml Lysozyme with 3 wt% of NaCl in D_2O at two different times during the crystallization process. Black lines: experimental data, Red lines: fit to the data. (For interpretation of the references to color in this figure legend, the reader is referred to the web version of this article.)

a protein solution, and at the final time t = 60.78 h, when a large lysozyme single crystal could be visible even by eyes. The first image shows a quite strong SANS signal around the beamstop and a scattering signal, probably coming from the glass capillary which contains the protein solution. No Bragg peak is visible at time t = 0.55 h, showing that no detectable crystals are present in the initial solution. In the second image, the intensity of the SANS signal is noticeably reduced and well distinct Bragg peaks are observed. These Bragg peaks are not moving during the crystallization process. This means that the growing crystal does not change its position during the crystallization process. Therefore, it cannot be ruled out that this crystal nucleated heterogeneously on the surface of the quartz capillary. The absence of Debye-Scherrer rings suggests that the crystallization process drove the protein solution to form a single crystal in the neutron beam.

4.1. SANS signal analysis

The obtained SANS curves at different times of the crystallization process are shown in Fig. 3. By comparing the two SANS curves at the beginning (left) and at the end (right) of the experiment it is possible to observe a decreasing signal intensity around the primary beam, which reflects a decrease of the lysozyme concentration in the solution. At the same time, the formation of a very pronounced single Bragg peak, around 0.34 $Å^{-1}$, within the integration box of the SANS signal can be observed. A similar behaviour for Lysozyme was suggested by Finet et al. [15]. However, because of the X-ray radiation damage, they could not study the temporal evolution of the SAXS curves from the same lysozyme solution. The experimental small angle scattering data has been fitted using the following expression, which takes account for the coherent differential cross section:

$$\frac{d\Sigma}{d\Omega} = N_{Lyso} v_o^2 (\rho_s - \rho_0)^2 f(Q) S(Q) + B \tag{5}$$

where ρ_0 and ρ_s are the calculated scattering lenght density of D_2O (ρ_0 = $0.06404 \cdot 10^{-12}$ cm $Å^{-3}$, $\rho_s = 0.00352 \cdot 10^{-12}$ cm $Å^{-3}$) and of the hydrogenated Lysozyme, respectively [8]. N_{Lyso} and $v_0 = 4\pi r^3/3$ are the number and the volume of Lysozyme objects, respectively. S(Q) is the structure factor, which has been assumed equal to 1, B is a constant background parameter and $f(Q) = A(Q)^2$ is the form factor of a perfect sphere, which is used here as an approximate description of the dissolved lysozyme molecules:

$$A(Q) = 3\left(\frac{sin(Qr) - (Qr)cos(Qr)}{(Qr)^3}\right) \tag{6}$$

The form factor $f(Q)$ takes account of the monomers and dimers [16] that cannot be distinguished here because of the noise present in the SANS signal. This is due to the fact that BIODIFF is not optimized to perform SANS measurements. The q-resolution δq of the instrument BIODIFF in the plotted q-range in Fig. 3 is between 0.018 $Å^{-1}$ and 0.025 $Å^{-1}$ taking into account a wavelength error of 3 % and a beam divergence of 0.7 ° (FWHM). This q-resolution is good enough to support the fitting of the N_{Lyso} parameter of Eq. 5, but it smears out the interference fringes described by the Eq. 6 leading only to a rough determination of the radius *r*. The radius *r* has been determined by a first fitting of the first SANS curve at t = 0.55 h, where also the N_{Lyso} and B were free parameters. Therefore, the fitted r_0 (the radius at t = 0.55 h) has been fixed during the fitting of all the following measurements. The r_0 was determined to be 14 Å. This result is close to the value of 15.8 Å, which is the equivalent radius of Lysozyme ($r_{eq} = \sqrt[3]{ab^2}$, where *a* and *b* are the semimajor and semiminor axes of the prolate ellipsoidal used to shape the lysozyme monomers in solution) measured with a SANS experiment by Chodankar et al. [17]. Apart from the limited q-resolution, this discrepancy between the two values could be ascribed both to a higher noise of the SANS curves measured here and the neglect of the dimers contribution. The observed number of Lysozyme scatterers was $1.1 \cdot 10^{17}$ cm^{-3} at the beginning and $5 \cdot 10^{16}$ cm^{-3} [1] at the end of the experiment. The temporal evolution of N_{Lyso} has been evaluated during the crystallization process and compared with the simultaneous integrated intensity of the [2,−1,4] Bragg peak observed by the neutron image plate (see yellow arrow in the Fig. 2). This Bragg peak was chosen because it shows a similar increase in intensity compared to other Bragg peaks. These results are shown in Fig. 5. The integrated intensity of the Bragg peak, was normalised to its highest value after the subtraction of the background intensity. The number of Lysozyme scatterers N_{Lyso} was also normalized to its highest value. Both curves resemble a sigmoid function even though a saturation point may not be completely achieved.

In order to determine how far away from the equilibrium the experiment is at t = 60.78 h, the crystallization process has been performed under the same conditions again (see Fig. 4). Here, the concentration of the Lysozyme was carefully measured using UV–vis spectroscopy. This enables the comparison of the Lysozyme concentration at t = 60.78 h with the solubility limit of Lysozyme as inferred from literature values. During the crystallization process, the growth rate of Lysozyme crystals depends on the degree of supersaturation value $\beta = P/S$, where *P* and *S* describe the initial protein concentration and the solubility at the same salt concentration, respectively [18–20]. The Lysozyme concentration decreases till the equilibrium (saturated solution) is achieved. At that point, when $\beta = 1$, the crystal growth stops and the consumption of the Lysozyme scatterers as well. The Lysozyme solubility in our experimental condition (pH of 4.75, at 298 K, NaCl 3 wt %) was found to be between 16 and 18 mg/ml [21]. As our experiment has been performed in D_2O, a temperature shift of 7.2 °C, [22] was taken into consideration, by using a known relation between the Lysozyme solubility in H_2O and D_2O. The Lysozyme concentration of the solution, measured by UV–vis spectroscopy, at the end of the experiment (t = 60.78 h) showed a value of 17 mg/ml, suggesting that the equilibrium point was nearly completely achieved and the dissolved Lysozyme scatterers do not contribute anymore to the crystal growth.

After almost 35 h, when generally the first crystals can be clearly seen by eyes, the two curves in Fig. 5 are crossing. At this time, the [2,−1,4] Bragg peak starts to be easily visible in the detector neutron image plate, showing the presence of a sufficient number of ordered lattice planes in the crystal. In the following hours, while the small angle scattering intensity decreases, the intensity of the integrated Bragg peak increases, suggesting a growing of the crystal size and so, the number of

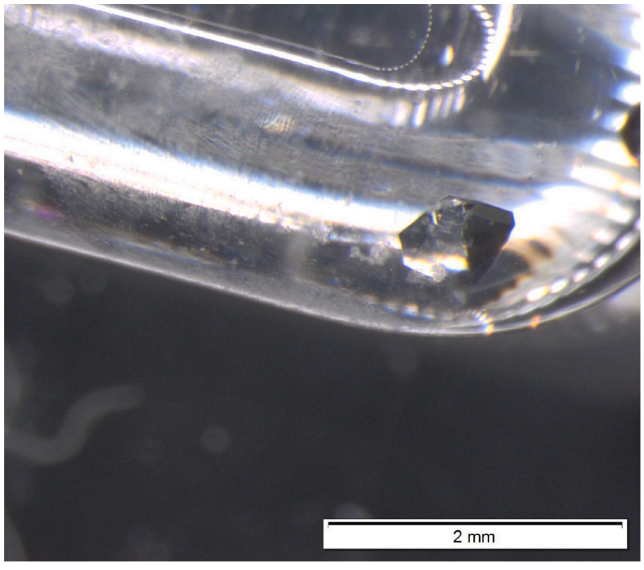

Fig. 4. Picture of the Lysozyme sample in experimental condition analogous to that used during the measuraments performed at BIODIFF at time t = 60.78 h.

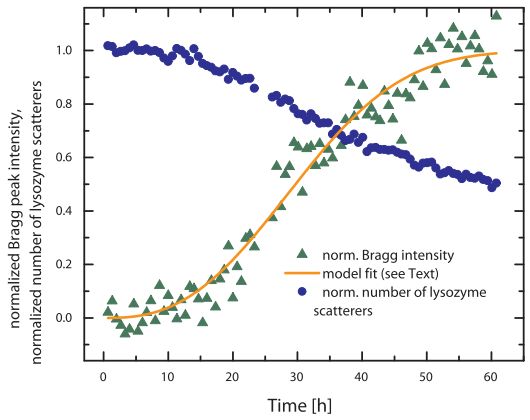

Fig. 5. Temporal evolution of the normalized intensity of a single integrated Bragg peak (green triangles) and the normalized number of the Lysozyme scatterers (blue circles). The solid orange line describes the fit the data obtained with the JMAK mode. (For interpretation of the references to color in this figure legend, the reader is referred to the web version of this article.)

the lattice planes. The decrease of the concentration of the lysozyme scatterers and the simultaneous appearing of the Bragg peak suggest that the lysozyme scatteres are consumed during the formation of nuclei and the crystal growth.

The temporal evolution of the [2,−1,4] Bragg peak integrated intensity has been interpreted by means of the Johnson-Mehl-Avrami-Kolmogorov (JMAK) model [23–26], which describes the time evolution of the fraction of transformed material during an isothermal crystallization. This model was already used to describe the crystallization kinetics for isothermal processes [27,17]. It is based on the assumption that during the crystallization the temperature is constant, the reaction proceeds by nucleation and growth and it assumes that the nucleation occurs randomly starting from spherical objects [23]. The first hypothesis is guaranteed by the experimental conditions, the second one is in agreement with our previous results [1], where a two-step crystallization process for the same model system was suggested. Finally, the third assumption is compatible with the homogeneous nucleation observed in our previous work [1]. The JMAK equation is described by the following relationship:

$$X(t) = 1 - e^{-k \cdot t^n} \tag{7}$$

where $X(t)$ is the fraction of the crystalline material as a function of time, k is an effective rate constant depending on the nucleation and growth rates and n is the so called Avrami exponent. The Avrami exponent is expected to be an integer or half integer value and depends on the characteristics of the process. For example, when a 3D spherical growth is assumed, the Avrami exponent is $n = 4$ [23]. It can also be described by the following relation [28,29]:

$$n = a + pN_{dim} \tag{8}$$

where a is equal to zero for existing nuclei (no nucleation occurs during the crystal growth) and to unity for a constant nucleation rate. N_{dim} represents the dimensionality of the crystal growth (N_{dim} is equal to 1 for 1D crystal growth, to 2 and 3 for 2D and 3D crystal growth, respectevely) and p is related to the growth mechanism ($p = 1$ for linear growth and $p = 1/2$ for diffusion controlled growth). By fitting the temporal evolution of the [2,−1,4] Bragg peak integrated intensity, we found out a value of $k = 9 \pm 4 \cdot 10^{-5}$ and $n = 2.6 \pm 0.1$. The Avrami exponent ($n \sim 2.5$) agrees with the assumption of a constant nucleation rate ($a = 1$), a final 3D crystal growth ($N_{dim} = 3$) and the diffusion limited cluster aggregation model observed for the crystal growth of the same system [1] (p = 1/2). A similar value for the Avrami exponent ($n = 2$) was found by Chodankar et al. [16] during the crystallization of Lysozyme at different concentrations of potassium bromide (KBr).

5. Conclusions

In this contribution we used the instrument BIODIFF both as a small angle scattering instrument and a high resolution neutron protein crystallography beam line at the same time. We could show that lysozyme crystallization proceeds under constant neutron flux over a long measurement duration underlining the fact that the nearly complete absence of radiation damage by neutrons makes them suitable for investigating biological samples. Since we evaluated both the small angle signal and the high resolution part of the detector image we could relate the consumption of lysozyme dimers with the crystal formation. Using the well-established JMAK model for crystallization we could derive the Avrami exponent for this process and a nucleation rate in combination with previous data. This contribution shows how neutron scattering can elucidate the crystallization process on the time scales of hours without the influence of radiation damage.

CRediT authorship contribution statement

M. Longo: Writing – original draft, Data curation, Visualization. **R.J. Heigl:** Resources, Writing – review & editing, Data curation, Investigation. **T.E. Schrader:** Writing – review & editing, Project administration, Supervision, Conceptualization, Funding acquisition.

Declaration of Competing Interest

The authors declare that they have no known competing financial interests or personal relationships that could have appeared to influence the work reported in this paper.

Acknowledgement

This project received funding from the European Union's Horizon 2020 research and innovation programme under Grant Agreement No. 654000.

References

[1] R.J. Heigl, M. Longo, J. Stellbrink, A. Radulescu, R. Schweins, T.E. Schrader, Cryst. Growth Des. 18 (2018) 1483–1494.
[2] S.C. Shoemaker, N. Ando, Biochemistry 57 (2018) 277–285.
[3] A. Sauter, F. Roosen-Runge, F.J. Zhang, G. Lotze, R.M.J. Jacobs, F. Schreiber, J. Am. Chem. Soc. 137 (2015) 1485–1491.
[4] Y. Georgalis, P.W.S. Umbach, B. Ihmels, S.D.M. Soumpasi, J. Am. Chem. Soc. 121 (1998) 1628–1635.
[5] P. Umbach, Y. Georgalis, W.S., J. Am. Chem. Soc. 120 (1998) 2383–2390.
[6] C. Beck, M. Grimaldo, F. Roosen-Runge, R. Maier, O. Matsarskaia, M. Braun, B. Sohmen, O. Czakkel, R. Schweins, F. Zhang, T. Seydel, F. Schreiber, Cryst. Growth Des. 19 (2019) 7036–7045.
[7] A. Ostermann, T.E. Schrader, J. Large-scale Res. Facil. 1 (2015) A2.
[8] J. Fitter, T. Gutberlet, J. Katsaras, Biol. Med. Phys. Biomed. Eng. 1 (2005) 1–549.
[9] R.P. May, K. Ibel, J.J. Haas, Appl. Cryst. 15 (1982) 15–19.
[10] Z. Otwinowski, W. Minor, Methods Enzymol. 276 (1997) 307–326.
[11] M.C. Vaney, S. Maignan, M. Ries-Kautt, A. Ducruix, Acta Cryst. D52 (1996) 505–517.
[12] C.A. Schneider, W.S. Rasband, K.W. Eliceiri, Nat. Methods 9 (2012) 671–675.
[13] P.J. Stothart, Appl. Cryst. 20 (1987) 362–365.
[14] S. Okabe, M. Nagao, T. Karino, S. Watanabe, T. Adachi, H. Shimizuc, M. Shibayama, J. Appl. Crystallogr. 38 (2005) 1035–1037.
[15] S. Finet, F. Bonnete, K.P. Frouin, A. Tardieu, Eur. Biophys. J. 27 (1998) 263–271.
[16] S. Chodankar, V.K. Aswal, Phys. Rev. E 72 (2005) 041931–041937.
[17] S. Chondankar, V. Aswal, J. Kohlbrecher, P. Hassan, A. Wagh, Phys. B 398 (2007) 164–171.
[18] M. Ataka, S. Tanaka, Biopolimers 25 (1986) 337–350.
[19] M. Ataka, Prog. Cryst. Growth Character. 30 (1995) 109–128.
[20] A. Elgersma, M. Ataka, T. Katsura, J. Cryst. Growth 122 (1992) 31–40.
[21] B. Howard, P.J. Twigg, J.K. Baird, E.J. Meehan, J. Cryst. Growth 90 (1988) 94–104.
[22] C. Gripon, L. Legrand, I. Rosenman, M.C. Vidal, F. Blue, J. Cryst. Growth 177 (1997) 238–247.
[23] W.A. Johnson, R. Mehl, Trans. AIME 135 (1939) 416.
[24] M.J. Avrami, Chem. Phys. 7 (1939) 1103.

[25] M.J. Avrami, Chem. Phys. 8 (1940) 212.
[26] M.J. Avrami, Chem. Phys. 9 (1941) 177.
[27] M. Zanatta, L. Cormier, L. Hennet, C. Petrillo, F. Sacchetti, Sci. Rep. 7 (2017) 43671.
[28] F.L. Cumbrera, F. Sanchez-Bajo, Thermochim. Acta 266 (1995) 315–330.
[29] A.M. Concerrado, I. Jagoba, J.L. Toca-Herrera, Microscopy Res. Technol. 81 (2018) 1095–1104.